Effect of postsynthesis preparation procedure on the state of copper in CuBEA zeolites and its catalytic properties in SCR of NO with NH3

Rafal Baran, Frederic Averseng, Dominik Wierzbicki, Karolina Chalupka, Jean-Marc Krafft, Teresa Grzybek, Stanislaw Dzwigaj

Effect of postsynthesis preparation procedure on the state of copper in CuBEA zeolites and its catalytic properties in SCR of NO with NH₃

Rafal Baran[1,2,3], Frederic Averseng[2,3], Dominik Wierzbicki[1], Karolina Chalupka[4], Jean-Marc Krafft[2,3], Teresa Grzybek[1], Stanislaw Dzwigaj[2,3,*]

[1]AGH University of Science and Technology al. A. Mickiewicza 30, 30-059 Krakow, Poland

[2]Sorbonne Universités, UPMC Univ Paris 06, UMR 7197, Laboratoire de Réactivité de Surface, F-75005, Paris, France

[3]CNRS, UMR 7197, Laboratoire de Réactivité de Surface, F-75005, Paris, France

[4]Lodz University of Technology, Institute of General and Ecological Chemistry, Zeromskiego 116, 90-924 Lodz, Poland
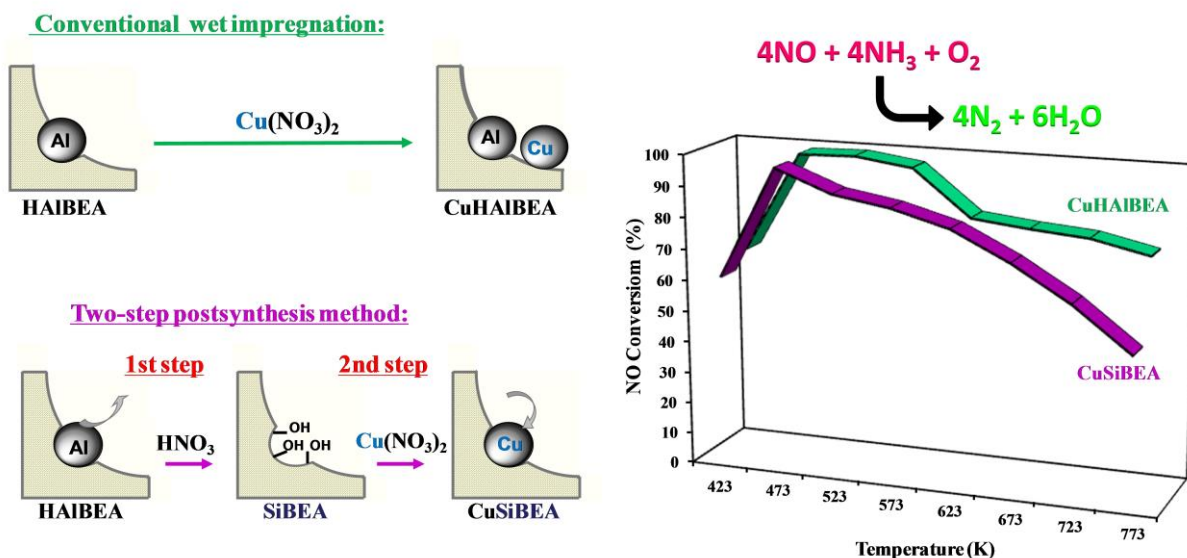
*Corresponding author:
Dzwigaj Stanislaw, E-mail : stanislaw.dzwigaj@upmc.fr, Fax : 33 1 44 27 21 13

Figures: 10

Tables: 4

Graphical abstract

Highlights

- **In Cu$_{2.0}$HAlBEA mainly extra-framework octahedral Cu(II) was present.**
- **In Cu$_{2.0}$SiBEA mainly framework mononuclear Cu(II) was occurred.**
- **Both Cu$_{2.0}$HAlBEA and Cu$_{2.0}$SiBEA catalysts showed high activity in SCR NO with NH$_3$.**
- **The state of copper as well as the acidity plays an important role in SCR of NO.**

Abstract

Copper-containing BEA zeolites, Cu$_{2.0}$SiBEA and Cu$_{2.0}$HAlBEA, with 2 wt % of Cu were prepared by a two-step postsynthesis method and a conventional wet impregnation, respectively. These zeolites were characterized by XRD, DR UV-vis, EPR, FTIR and TPR physicochemical techniques. The incorporation of Cu into framework of SiBEA was evidenced by XRD. The state of copper in both zeolites was investigated by DR UV-vis and EPR. The acidity of Cu$_{2.0}$SiBEA and Cu$_{2.0}$HAlBEA was determined by FTIR of adsorbed CO and pyridine. The reducibility of the Cu species present in both zeolites was studied by TPR and their catalytic properties were investigated in selective catalytic reduction of NO with

NH_3. Both $Cu_{2.0}SiBEA$ and $Cu_{2.0}HAlBEA$ zeolite catalysts showed very high activity in this reaction with the NO conversion higher than 80 % and N_2 selectivity higher than 95 % in the temperature range between 473 and 623 K. The higher NO conversion and N_2 selectivity in SCR of NO with ammonia at the high temperature range for the $Cu_{2.0}HAlBEA$ than for $Cu_{2.0}SiBEA$ suggest that the strong Brønsted and Lewis acidic sites related to the framework and extra-framework aluminum atoms play an important role in SCR of NO process.

Keywords: Copper, Beta zeolites, NH_3, SCR of NO

1. Introduction

Copper containing zeolites have been extensively tested in selective catalytic reduction of NO with ammonia. Especially high activity and selectivity to N_2 were reported for Cu-ZSM-5 and Cu-BEA zeolites [1–4]. However, recently, zeolites with smaller pores size, such as SSZ-13 and SAPO-34, have been indicated as the most promising materials for application in diesel systems SCR unit due to high chemical and thermal stability [5–8]. Nevertheless, further development in catalytic NO_x abatement technologies is necessary due to severe environmental regulation related to nitrogen oxides emission.

The main obstacles leading to deactivation of copper containing zeolites are hydrothermal dealumination and poisoning of active species as well as migration and sintering of copper species over SCR process. A possible solution of those issues is the improvements in catalysts preparation methods. An optimal catalyst preparation procedure should allow controlling the speciation of active sites and to obtain isolated species well fixed to support. Currently used conventional methods, such as ion-exchange and impregnation, leads to introduction of active species in various forms i.e. isolated framework species, isolated cations in exchange positions and extra-framework nanoclusters.

Some of scientists involved in $DeNO_x$ processes proposed a direct synthesis of Cu containing zeolites by the addition of organo-copper complexes in the synthesis gel as an alternative method to conventional ion exchange and impregnation [9]. However, this kind of method resulted in undesired mixture of copper in framework and extra-framework positions.

On the other hand, Dzwigaj et al. [10–12] have proposed a new method for postsynthesis modification of beta zeolite which consists of two steps. In the first step, vacant T-atom sites are created by treatment of parent zeolite with nitric acid solution. In the second

step, the metal ions react with silanol groups of vacant T-atom sites forming framework metal species with well-defined environment.

In this work it was studied the influence of two different catalyst preparation procedures, conventional wet impregnation and two-step postsynthesis method, on the nature and environmental of copper introduced in $Cu_{2.0}HAlBEA$ and $Cu_{2.0}SiBEA$, respectively. Moreover, both copper containing catalysts were applied for selective catalytic reduction of NO with ammonia and their performances were compared.

2. Experimental Section

2.1. Materials

Copper-containing BEA zeolites (with 2 Cu wt %) were prepared from parent TEABEA zeolite by a two-step postsynthesis method ($Cu_{2.0}SiBEA$) and a conventional wet impregnation ($Cu_{2.0}HAlBEA$) using SiBEA and HAlBEA as the supports whose preparation was described in our earlier work [13].

$Cu_{2.0}SiBEA$ and $Cu_{2.0}HAlBEA$ were prepared by impregnation of 2 g of SiBEA and HAlBEA, respectively, with $Cu(NO_3)_2 \cdot 6H_2O$ solutions with appropriate concentration of copper. Firstly, the suspensions were stirred for 24 h at 298 K in excess solvent using 200 mL of the precursor solutions. Then, the suspensions were stirred in evaporator under vacuum of a water pump in air at 353 K for 2 h until water was evaporated. $Cu_{2.0}SiBEA$ and $Cu_{2.0}HAlBEA$ were calcined in air (100 K h^{-1}) at 773 K for 3 h under static condition and labeled as C-$Cu_{2.0}SiBEA$ and C-$Cu_{2.0}HAlBEA$, respectively, where C- stands for calcined.

2.2. Techniques

X-ray Fluorescence chemical analysis was performed at room temperature on SPECTRO X-LabPro apparatus.

Copper-containing beta zeolites were investigated by chemical analysis, powder X-ray diffraction (XRD), diffuse reflectance UV-vis (DR UV-vis), electron paramagnetic resonance (EPR), Fourier transform infrared spectroscopy combined with CO sorption (CO-FTIR) and temperature programmed reduction (TPR).

XRD experiments were carried out on a PANalitical Empyrean diffractometer using the CuK$_\alpha$ radiation ($\lambda = 154.05$ pm). All experiments were performed at room temperature.

DR UV–vis spectra were recorded at ambient atmosphere on a Cary 5000 Varian spectrometer equipped with a double integrator with polytetrafluoroethylene as reference.

EPR spectra were recorded on a JEOL FA-300 series EPR spectrometer at about 9.3 GHz (X band) using a 100-kHz field modulation and a 5−10 G standard modulation width. The spectra were recorded at 298 and 77 K. Simulations were performed using the EPRSim32 software developed by Spalek et al [14].

Analysis of the acidic properties of samples by adsorption of pyridine (Py) followed by infrared spectroscopy was performed in the same way as is described in [15].

Infrared spectroscopy of CO adsorption/desorption experiments was performed on a Bruker Vertex 70 spectrometer. Before analysis, self-supported samples were pressed at ca. 1 ton cm^{-2} into thin wafers of ca. 10 mg cm^{-2} and set inside the glass cell where they were pre-treated at 723 K for 2 h in flowing 2.5 % O_2/Ar and then degassed at 573 K (10^{-3} Pa) for 1 h.

Finally, IR cell was cooled down to 100 K with liquid nitrogen, and CO was added in small portions up to an equilibrium pressure of 133 Pa. Then, the sample was evacuated up to 10^{-3} Pa at room temperature. The spectra were obtained after subtraction of the spectrum recorded before CO adsorption.

The H_2-TPR measurements were carried out on an AutoChem 2910 apparatus (Micromeretics) equipped with a thermal conductivity detector (TCD) in the temperature range of 298−900 K with a linear heating rate of 7 K min^{-1}, hydrogen stream (5 % H_2/Ar) flow of 40 cm^3 min^{-1} and samples weight of 0.1 g. The copper reduction degree in C-$Cu_{2.0}$SiBEA and C-$Cu_{2.0}$HAlBEA were calculated in following way. From sample mass and Cu content were calculated the number of Cu mole and theoretical number of H_2 moles which are needed to reduce Cu:

$$n_{Cu} = n_{H_2(t)} = \left(\frac{C_{Cu} \times m_s}{100\ \%} \right) \Big/ M_{Cu}$$

where n_{Cu} is number of Cu mole in the sample, $n_{H2(t)}$ is number of H_2 moles need to completely reduce Cu in sample, m_s is sample mass and M_{Cu} is molar mass of Cu. From total area under the reduction peaks of standard CuO and the samples were calculated the number of H_2 moles consumed to reduce Cu:

$$n_{H_2(r)} = S_s \times n_{H_2(CuO)} \Big/ S_{CuO}$$

where: $n_{H2(r)}$ and S_s are the number of H_2 mole consumed for Cu reduction and total area under reduction peaks for the zeolite samples, respectively, $n_{H2(CuO)}$ is the number of H_2 mole used for reduction of pure CuO and S_{CuO} is the total area of reduction peak, calculated for pure CuO (standard). Reduction degree of Cu in samples was calculated form equation:

$$R_{Cu} = {n_{H_2(r)}}/{n_{H_2(t)}} \times 100\ \%$$

where R_{Cu} is copper reduction degree.

The activity tests of $Cu_{2.0}SiBEA$ and $Cu_{2.0}HAlBEA$ catalysts in selective catalytic reduction (SCR) of NO with ammonia were performed in a fixed bed reactor. The composition of the reaction gas was: 1000 ppm NO, 1000 ppm NH_3, 3.5 vol. % O_2 and He as balance. The gas mixture was provided with calibrated electronic mass flow controllers (BETA-ERG). The total gas flow was 0.1 L min^{-1} and catalyst mass was 0.2 g. The concentrations of NO and N_2O after reaction were analyzed by FTIR detectors (ABB 2020 AO series). Prior to the reaction the catalyst bed was activated in 3.5 % O_2/He flow (0.1 L min^{-1}) in the temperature range of 298–798 K with a linear heating rate of 2 K min^{-1} and then for 1 h at 798 K. The standard test was carried out over 1 h at 573–773 K with increasing reaction temperature every 50 K interval. The NO conversion was calculated from the measured concentration of nitrogen oxide.

3. Results and Discussion

3.1. Incorporation of copper into zeolite framework determined by XRD and FTIR

3.1.1. X-ray diffraction

The experiments of chemical analysis of zeolite samples allowed determine the Si/Al ratio and Cu content and the results are showed in **Table 1**.

Both $Cu_{2.0}HAlBEA$ and $Cu_{2.0}SiBEA$ zeolites are characterized by similar XRD patterns as that of HAlBEA and SiBEA supports (**Fig. 1**). It indicates that introduction of copper into both type of BEA supports did not affect crystal structure of these materials. The observations of the zeolites XRD patterns before and after introduction of copper (**Fig. 1**) showed that for HAlBEA only negligible shift of the main diffraction peak was observed from $2\theta = 22.45°$ to $2\theta = 22.39°$ after introduction of copper by conventional wet impregnation. However, for the SiBEA significant shift of the main diffraction peak is observed (from $2\theta = 22.72°$ for SiBEA to $2\theta = 22.59°$ for $Cu_{2.0}SiBEA$) after introduction of copper by the two-step postsynthesis method. It suggests that upon the latter preparation method copper was incorporated into framework of BEA zeolite by reaction with silanol groups of vacant T-atom sites formed in the first step of this procedure as a result of the removal of Al upon nitric acid treatment, in line with earlier investigations on CuSiBEA materials [16,17]. Moreover, for the used catalysts differences in their XRD patterns are clearly seen. For spent-$Cu_{2.0}SiBEA$ a large shift of the main diffraction reflection (from 22.72° for SiBEA to 22.28° for spent-$Cu_{2.0}SiBEA$) was observed indicating that sample activation and reaction conditions led to

strong incorporation of copper species into SiBEA zeolite framework. In contrast, for spent-$Cu_{2.0}$HAlBEA the position of the main diffraction peak is almost the same as for HAlBEA support, it suggest that in the case of latter support the copper was not incorporated in the zeolite framework and was predominantly present in extra-framework position.

3.1.2. FTIR

The FTIR spectra of HAlBEA $Cu_{2.0}$HAlBEA, SiBEA and $Cu_{2.0}$SiBEA are shown in the **Figure 2**. The spectra for HAlBEA and SiBEA supports were thoroughly described in our earlier works on BEA zeolites [13,18]. The introduction of 2 % of Cu into HAlBEA led to disappearance of broad band at 3550 cm^{-1}, narrow band at 3781 cm^{-1} and decrease in the intensity of the band at 3608 cm^{-1} suggesting that cooper ions interacts with corresponding hydroxyl groups and some part of H^+ was exchanged with Cu^{2+} in cationic positions of HAlBEA zeolite.

The treatment of organic-free BEA zeolite with high concentrated nitric acid solution leads to removal of aluminum species and appearance in the spectrum of SiBEA the intense bands at 3735 and 3520 cm^{-1} of SiO-H groups (**Fig. 2**) due to the formation of vacant T-atom sites with hydrogen-bonded silanol groups, as reported earlier [19]. The impregnation of SiBEA with aqueous solution of cooper precursor resulted in strong decreasing of intensity of OH bands of hydrogen bonded silanol groups at 3520 cm^{-1} (**Fig. 2**) suggesting that Cu(II) reacted with these silanol groups leading to the incorporation of copper ions into framework of SiBEA.

3.2. Nature of copper determined by DR-UV-vis and EPR

In order to describe the chemical nature and the environment of copper in C-$Cu_{2.0}$SiBEA and C-$Cu_{2.0}$HAlBEA the DR UV-vis and EPR spectroscopies were used.

3.2.1. DR UV-vis spectroscopy

DR UV-vis spectra of $Cu_{2.0}$HAlBEA and $Cu_{2.0}$SiBEA samples contained d-d transition bands at approximately 835 nm and an intense charge-transfer (CT) band at 280 nm (**Fig. 3**). These bands could be assigned to the d-d transition of Cu^{2+} ($3d^9$) and CT $O^{2-} \rightarrow Cu^{2+}$ transition of isolated mononuclear Cu(II) being in coordination with lattice oxygen, respectively [20–23]. The absence of the DR UV-vis band in the range of 300-600 nm assigned to O^{2-} to Cu^{2+} charge-transfer transition of dinuclear [20,21,24] or trinuclear [24,25] copper-oxygen complex for $Cu_{2.0}$SiBEA indicates that such polynuclear complexes were not present in the latter sample. For $Cu_{2.0}$HAlBEA additionally a DR UV-vis band at 400 nm

occurred typical for octahedral Cu(II) species [20,21,24,25], suggesting the presence of such species in this sample.

Calcination of both $Cu_{2.0}HAlBEA$ and $Cu_{2.0}SiBEA$ samples at 773 K for 3 h leads to important changes in the DR UV-vis spectra. The spectra of C-$Cu_{2.0}HAlBEA$ and C-$Cu_{2.0}SiBEA$ are composed of a broad band at around 780-785 nm (**Fig. 3**) attributed to d-d transition of Cu(II) ($3d^9$) and the bands at around 340 and 315 nm (**Fig. 3**), related to oxygen-to-copper(II) charge transfer (CT) transitions involving framework oxygen and copper present in the zeolite structure as extra-framework octahedral Cu(II) and framework mononuclear Cu(II), respectively, in line with earlier reports [20,26,27].

According to DR UV-Vis results it may be concluded that for C-$Cu_{2.0}HAlBEA$ catalyst copper predominantly occurred as octahedral Cu(II) species, whereas for C-$Cu_{2.0}SiBEA$ mainly as isolated mononuclear Cu(II) species.

3.2.2. Electron Paramagnetic Resonance spectroscopy

The EPR spectrum of $Cu_{2.0}HAlBEA$ sample obtained at 298 K (**Fig. 4**) shows a broad, featureless and slightly anisotropic signal (axial symmetry). Due to its broadness, its $g_\parallel$ and $g_\perp$ values can only be estimated. The averaged value of this signal ($g_{aver.} = 1/3(g_\parallel + 2\ g_\perp) = 2.20$) is close to that observed earlier [28–32] for hydrated octahedral Cu(II) species exhibiting rotational/mobility freedom or a quick change of the elongation axis. Upon cooling down to 77 K, the EPR signal transforms to an axial one presenting hyperfine splitting ($A_\parallel$) (**Fig. 5**). The simulated EPR parameters (see Table 1) are very similar to those previously published for CuZSM-5 and Cu-BEA samples [29,32–35], and can be assigned to hydrated octahedral Cu(II) species for which the mobility/motion has been severely reduced at 77 K.

As showed in **Fig. 4,** calcined C-$Cu_{2.0}HAlBEA$ sample exhibits at 298 K a similar EPR signature as that of $Cu_{2.0}HAlBEA$, with an additional weak signal (shoulder around g = 2.08 in **Fig. 4**) that may be assigned to hydrated octahedral immobilized Cu(II) species. Such immobilization could be explained by removal upon calcination of water ligands and formation strong Cu-$O_{lattice}$ bond. At 77 K, the EPR spectrum is very similar to that obtained for $Cu_{2.0}HAlBEA$ but more intense and better resolved.

In the case of $Cu_{2.0}SiBEA$ sample, the EPR signal obtained at 298 K is featureless and isotropic ($g_{iso} = 2.19$) (**Fig. 4**), once again typical of hydrated octahedral Cu(II) species, but with a higher motional freedom than that observed for $Cu_{2.0}HAlBEA$. This is confirmed by

the spectrum recorded at 77 K (**Fig. 5**) when a large portion of mobile hydrated octahedral Cu(II) species is still observed.

Upon calcination of $Cu_{2.0}$SiBEA sample, the Cu(II) signals recorded for C-$Cu_{2.0}$SiBEA at 298 K (**Fig. 4**) and 77 K (**Fig. 5**) decreased in intensity, pointing out that a big portion of copper species has become EPR silent. The remaining EPR signal correspond to hydrated octahedral Cu(II) species mainly immobilized or frozen with a small portion of mobile ones only present at 298 K (see **Table 2** for EPR parameters). Such strong decrease of overall EPR signal intensity has been frequently reported in the literature for Cu-containing zeolites, especially after outgassing/dehydration [28–30,36–38]. Three possible causes may explain such EPR intensity drop: (i) reduction of Cu(II) to diamagnetic Cu(I) species; (ii) formation of Cu(II)-O-Cu(II) species (O referring either to O_2^- or OH^-) or (iii) transformation of octahedral Cu(II) species into lower coordinated Cu(II) ones, especially into slightly distorted C_{3v} trigonal symmetry. In the third case, such Cu(II) species present very close low lying excited states allowing for a very fast spin-lattice relaxation and resulting in large broadening and the associated loss in intensity of the EPR signal so that it may not be observable even at 77 K.

As $Cu_{2.0}$SiBEA being calcined in air, the reduction of Cu(II) to Cu(I) species seems unlikely. Also, a good dispersion of Cu(II) species upon preparation of $Cu_{2.0}$SiBEA by two-step postsynthesis method and the low Cu content may rule out the formation of Cu(II)-O-Cu(II) species or magnetically interacting Cu(II) centers. A possible explanation of the strong decrease of the EPR signal intensity for C-$Cu_{2.0}$SiBEA sample would be the formation of a large amount of isolated and EPR-silent Cu(II) species with specific C_{3v} symmetry. Such species would result from the incorporation of copper in the framework of SiBEA zeolite by reaction with silanol groups of hydroxyl nests created during removal of aluminium from the zeolite upon acid nitric treatment.

3.3. Acidity of $Cu_{2.0}$HAlBEA and $Cu_{2.0}$SiBEA determined by FTIR + CO
3.3.1. FTIR + CO

The FTIR spectroscopy following CO sorption as a probe molecule was applied in order to study the acidic centers present in both $Cu_{2.0}$HAlBEA and $Cu_{2.0}$SiBEA zeolites. It is well known that CO molecules are more strongly bonded with Cu^+ than Cu^{2+} ions, however at low temperature it is possible to observe in the FTIR spectra bands related to both Cu(I) and Cu(II) species.

The adsorption of CO on $Cu_{2.0}HAlBEA$ zeolite led to appearance of bands at 2232, 2223, 2201, 2195, 2188, 2173, 2169, 2152, 2141, 2131 and 2131 cm^{-1} (**Fig. 6A**). Intensity of all bands gradually increased with addition of following CO doses. The two bands with highest wavenumbers at 2232 and 2223 cm^{-1} are due to interaction of CO with framework and extra-framework Al(III) species, in agreement with earlier report on BEA zeolite [39]. The very intense band at 2173 cm^{-1} is related to the adsorption of CO on bridged Si–O(H)–Al groups possesses strong acidic character [40]. Ascription of remaining bands to particular species is not easy because of their similar wavenumber positions in infrared spectra. In the previous investigations of Cu containing materials it was reported that mononuclear Cu(I) species might form with carbon monoxide mono-, di- and tricarbolyls moieties depending of temperature, CO pressure and environment of copper centers [41–44]. In the spectrum of $Cu_{2.0}HAlBEA$ the bands at 2152 and 2188 cm^{-1} may correspond to $Cu^{+}(CO)_2$ species and bands at 2195, 2169, 2141 cm^{-1} may be ascribed to $Cu^{+}(CO)_3$ species present in cationic positions consistent with similar observations of Bordiga et al. and Lamberti et al. [41,45]. Moreover, the high intensity of band at 2169 cm^{-1} may result from overlapping the band related to copper species by band related to SiO-H [46] which presence cannot be excluded. In line with recent studies [37,41], band at 2201 cm^{-1} represent Cu(II)-CO adducts, where CO is adsorbed on isolated copper (II) species. Gora-Marek et al. [47] indicated appearance of 2122 cm^{-1} bands as a result of weak Cu(0)-CO interactions, however due to the application of the oxidative atmosphere for sample pre-treatment we rather opted for Giordanino et al. [48] explanation, in which they attributed this band to interaction of CO with extra-framework Cu(I) species.

After introduction of CO up to 133.3 Pa (equilibrium pressure) gradual evacuation was performed as showed in **Figure 6B**. It can be seen that the evacuation led to complete disappearance of the bands at 2193, 2173, 2169, 2140 and 2136 cm^{-1} and a sharp decrease in the intensity of the bands at 2233, 2224, and 2200 cm^{-1}. Furthermore, at low CO coverage (inset **Fig. 5B**) the band at 2183 cm^{-1} became clearly visible and the band at 2152 cm^{-1} strongly developed during evacuation suggesting a transformation of tricarbonyl into dicarbonyl species, in line with earlier report [41]. It is important to stress that the Cu(II)-CO adducts were present even after the deep evacuation indicating considerable acidic character of Cu(II) species.

FTIR spectra of $Cu_{2.0}SiBEA$ zeolite after adsorption of CO exhibit nine bands (**Fig. 7A**). The most intense one at 2202 cm^{-1} is due to presence of isolated mononuclear copper(II) species, whereas bands at 2189, 2168 and 2140 cm^{-1} are related to $Cu^{+}(CO)_3$ species in

agreement with literature data [45]. Moreover the bands at 2129 and 2135 cm^{-1} are ascribed to copper(I) oxo-species in line with earlier reports on copper containing materials [49]. The bands at 2175, 2163 and 2161 cm^{-1} are related to acidic bridging hydroxyls, internal and external silanol groups, respectively, in line with earlier studies [40,46].

Upon evacuation, it was observed complete disappearance of the bands related to hydroxyls groups and tricarbonyls species. Simultaneously, the band at 2151 cm^{-1}, typical for Cu(I)-(CO)$_2$, appeared. Additionally, the band at 2135 cm^{-1}, which corresponds to relatively stable interaction between CO and Cu(I) of extra-framework copper compounds, was shifted to 2141 cm^{-1}. These results suggest similar interaction strength of Cu(II) and Cu(I) species with CO in Cu$_{2.0}$SiBEA. The significant intensity of the band at 2205 cm^{-1} after evacuation (inset **Fig. 7B**) may be due to stable and strong interaction between CO sorption on isolated framework Cu(II) species. Furthermore, for both studied zeolite the bond at 2157 cm^{-1}, related to the monocarbonyl species [43] which normally form after CO adsorption on isolated Cu$^+$, was not observed even after deep evacuation.

To sum up it may be said that in Cu$_{2.0}$SiBEA and Cu$_{2.0}$HAlBEA zeolite occur alternative copper species – mostly copper ions in the cationic positions for Cu$_{2.0}$HAlBEA zeolite and predominantly mononuclear framework Cu(II) species for Cu$_{2.0}$SiBEA zeolite.

3.3.2. FTIR + Pyridine

To precisely calculate concentration of acidic sites in supports and copper containing catalysts the FTIR experiments with pyridine adsorption were carried out for all studied samples. The results obtained after pyridine desorption at 423 K were summarized and compared in **Table 3**.

As we have recently evidenced [13], SiBEA contains very small amount of the Brønsted and Lewis acidic centers due to presence of traces of aluminum species remaining after nitric acid treatment. After the introduction of copper into SiBEA an increase in the number of Lewis acidic centers was observed (form 3 to 52 μmol g^{-1}), probably due to formation of isolated, framework copper(II) species. No formation of an additional amount of the Bronsted acidic sites was reported.

On the other hand, HAlBEA and Cu$_{2.0}$HAlBEA zeolites contained a large amount of acidic sites. However, after impregnation of HAlBEA support with the copper precursor the number of strong Bronsted sites decreased with simultaneous increase in amount of Lewis centers (**Table 3**). This effect was a result of partial exchange between Cu^{2+} and H$^+$ ions at the

cationic positions in BEA zeolite cavities. Thus, copper occurring in extra-framework positions resulted in formation of additional amount of Lewis acidic centers.

3.4. Reducibility of copper determined by TPR of H_2

TPR experiments were carried out to distinguish reducibility of different copper species present in C-$Cu_{2.0}$HAlBEA and C-$Cu_{2.0}$SiBEA samples. **Figure 8** exhibits TPR patterns of copper containing zeolites beta prepared with two different methods. TPR pattern of C-$Cu_{2.0}$HAlBEA exhibits quite broad two peaks at 535 and 690 K probably related to two steps reduction of copper (II) species, firstly from Cu(II) to Cu(I), and secondly from Cu(I) to metallic copper. Similar TPR results were observed for many other copper containing zeolites like Cu/SAPO-5, Cu-Beta and Cu-MFI [50–52]. However, broad character of both peaks may indicate presence of different copper species, not only mononuclear Cu(II) species but also more complex polynuclear Cu(II) species [43].

The TPR pattern of C-$Cu_{2.0}$SiBEA was significantly different compare to the pattern of C-$Cu_{2.0}$HAlBEA. It exhibits narrow peak at 490 K with a small shoulder at 465 K and additional low intense peak at 585 K. The signals at 465 and 490 K probably correspond to the reduction of Cu(II) to Cu(I) of two types mononuclear, framework copper species. The presence of two types of copper framework species is related to the appearance of two types of aluminum framework in the parent BEA zeolite [13,53].

The low intense peak with a maximum at 585 K may arise from the partial reduction of Cu(I) species to Cu(0). Low integral area of this signal may suggest that the reduction of Cu(I) species to metallic form was not complete, as a result of a strong interaction between SiBEA support and copper.

In order to confirm this statement, it was done the quantitative analysis of TPR results. As shown in **Table 4** copper in C-$Cu_{2.0}$HAlBEA was completely reduced whereas for C-$Cu_{2.0}$SiBEA only 65 % of Cu(II) reduction was achieved. It indicates that copper(II) in former catalyst reduces easier to metallic form. On the other hand, copper(II) species in C-$Cu_{2.0}$SiBEA are stronger coupled to the SiBEA matrix and they may remain as Cu(I) species in large contribution even after reduction at high temperature. Thus, these facts prove different nature and properties of copper species in the framework and extra-framework positions.

3.5. Catalytic activity of $Cu_{2.0}HAlBEA$ and $Cu_{2.0}SiBEA$ catalysts

In some of the previous reports [20,54–57] it was mentioned that in NO abatement reactions such as NO decomposition and HC-SCR of NO, the active centers were copper species present in zeolites cationic positions. The authors suggested that presence of aluminum in the zeolites framework is required in order to obtain active and high selective catalysts. Moreover, in the recent works on the most promising NH_3-SCR catalysts (Cu-SSZ and Cu-SAPO-34) it was indicated that Cu(II) species localized at 6-MR position of CHA structure and coordinated with two framework Al atoms are the most effective catalytic sites in NO reduction with ammonia [58–60].

After careful analysis of physicochemical properties of $Cu_{2.0}HAlBEA$ and $Cu_{2.0}SiBEA$ zeolites the catalytic tests of SCR of NO with ammonia were carried out to investigate the influence of preparation procedures on the catalysts activity and selectivity in DeNOx process. Moreover, the aim of our work was to compare behavior of extra-framework octahedral Cu(II) species predominantly present in $Cu_{2.0}HAlBEA$ with isolated framework mononuclear Cu(II) species occurring mainly in $Cu_{2.0}SiBEA$.

Figure 9 exhibits the NO conversion in NH_3-SCR on $Cu_{2.0}HAlBEA$ and $Cu_{2.0}SiBEA$ catalysts. At the low temperature range both catalysts gave almost the same NO conversion (~60 % at 423 K and ~95 % at 472 K). However, when the reaction temperature started to increase gradual decrease in the NO conversion was observed for $Cu_{2.0}SiBEA$, whereas for $Cu_{2.0}HAlBEA$ the activity remained very high (almost 100% of NO conversion) up to 573 K. Although in the higher temperature range both catalysts lost some activity. For $Cu_{2.0}SiBEA$ decrease in the catalytic activity was more significant than for $Cu_{2.0}HAlBEA$ (around 15 and 20 % lower NO conversion at 723 and 773 K for $Cu_{2.0}SiBEA$ than for $Cu_{2.0}HAlBEA$, respectively).

Furthermore, the N_2 selectivity (**Fig. 10**) was high for both catalysts in the whole temperature range. Slightly decrease in the selectivity toward N_2 with increasing reaction temperature was observed from 573 to 723 K. The N_2 selectivity did not drop to less that 90 % at any studied temperature. However, for $Cu_{2.0}HAlBEA$ it was slightly higher than for $Cu_{2.0}SiBEA$. In case of $Cu_{2.0}HAlBEA$ particular performance was observed at 423 – 573 K, when the N_2 selectivity was around 100 %. A small drop in selectivity toward N_2 might result from the presence of competitive reactions of the ammonia oxidation to NO and/or N_2O. NH_3 oxidation is especially strongly promoted by octahedral Cu(II) species at the high temperature range, in agreement with earlier works on the application of copper containing zeolites for NH_3-SCR process [61,62].

13

The better catalytic properties of $Cu_{2.0}HAlBEA$ than $Cu_{2.0}SiBEA$ may suggest that the vicinity of Al species improved catalytic activity of copper species leading to a bit higher activity and selectivity. However, the presence of aluminum in the framework is not necessary to obtain the efficient zeolite catalyst for NO removal, as it is showed by very high activity of $Cu_{2.0}SiBEA$. A slightly higher activity of $Cu_{2.0}HAlBEA$ than $Cu_{2.0}SiBEA$ at might be related to the presence in former much higher amount of strong Brønsted and Lewis acidic sites which may play important role in SCR mechanism according to the reports of Eng and Bartholomew [63] and Stevenson et al. [64]. As we described previously HAlBEA support contains a large amount of acidic centers, whereas SiBEA support possesses only a very little amount of acidic centers, as reported earlier [65].

The catalysts stability and activity in the presence of water steam in substrates stream were also studied. The results showed in **Figure S1** indicate that presence of water resulted in lower NO conversion, however catalyst stability remained high even after three catalytic cycles. More results about catalyst stability and comparison of our catalysts activity with literature data may be found in supportive information to this article (Table S1).

Conclusions

Modifications of zeolite beta by two different methods led to obtaining two types of catalysts with considerable different nature and environment of copper species.

Copper species in $Cu_{2.0}HAlBEA$ zeolite, prepared with conventional wet impregnation method, were predominantly present as extra-framework octahedral Cu(II) species, whereas copper species in $Cu_{2.0}SiBEA$ zeolite, obtained by two-step postsynthesis method, occurred mostly as framework mononuclear Cu(II) species.

Both $Cu_{2.0}SiBEA$ and $Cu_{2.0}HAlBEA$ zeolite catalysts showed a very high activity in this reaction with NO conversion higher than 80 % and N_2 selectivity higher than 95 % in the temperature range between 473 and 623 K.

However, catalyst prepared with conventional wet impregnation method gave better activity in NO conversion and N_2 selectivity in SCR of NO with ammonia at the high temperature range suggesting a positive effect of the aluminum atoms on catalyst performance in SCR of NO. Thus, it shown that the state of copper species as well as the acidity plays an important role in SCR of NO process.

References

[1]   N. Wilken, K. Wijayanti, K. Kamasamudram, N.W. Currier, R. Vedaiyan, A. Yezerets, L. Olsson, Appl. Catal. B Environ. 111-112 (2012) 58–66.

[2]   O. Mihai, C.R. Widyastuti, S. Andonova, K. Kamasamudram, J. Li, S.Y. Joshi, N.W. Currier, A. Yezerets, L. Olsson, J. Catal. 311 (2014) 170–181.

[3]   A. Corma, A. Palomares, F. Marquez, J. Catal. 139 (1997) 132–139.

[4]   S. Yashnik, Z. Ismagilov, Appl. Catal. B Environ. 170-171 (2015) 241–254.

[5]   I. Lezcano-Gonzalez, U. Deka, H.E. van der Bij, P. Paalanen, B. Arstad, B.M. Weckhuysen, A.M. Beale, Appl. Catal. B Environ. 154-155 (2014) 339–349.

[6]   L. Ma, Y. Cheng, G. Cavataio, R.W. McCabe, L. Fu, J. Li, Chem. Eng. J. 225 (2013) 323–330.

[7]   A. Shishkin, H. Kannisto, P.-A. Carlsson, H. Härelind, M. Skoglundh, Catal. Sci. Technol. 4 (2014) 3917–3926.

[8]   J.H. Kwak, R.G. Tonkyn, D.H. Kim, J. Szanyi, C.H.F. Peden, J. Catal. 275 (2010) 187–190.

[9]   R. Martínez-Franco, M. Moliner, P. Concepcion, J.R. Thogersen, A. Corma, J. Catal. 314 (2014) 73–82.

[10]   S. Dzwigaj, M. Matsuoka, R. Franck, M. Anpo, M. Che, J. Phys. Chem. B 102 (1998) 6309–6312.

[11]   S. Dzwigaj, M. Che, J. Phys. Chem. B 110 (2006) 12490–3.

[12]   S. Dzwigaj, T. Shishido, J. Phys. Chem. C 112 (2008) 5803–5809.

[13]   R. Baran, Y. Millot, T. Onfroy, J.M. Krafft, S. Dzwigaj, Microporous Mesoporous Mater. 163 (2012) 122–130.

[14]   T. Spałek, P. Pietrzyk, Z. Sojka, J. Chem. Inf. Model. 45 (2005) 18–29.

[15]   A. Śrebowata, R. Baran, D. Łomot, D. Lisovytskiy, T. Onfroy, S. Dzwigaj, Appl. Catal. B Environ. 147 (2014) 208–220.

[16]   S. Dzwigaj, J. Janas, J. Gurgul, R.P. Socha, T. Shishido, M. Che, Appl. Catal. B Environ. 85 (2009) 131–138.

[17]   J. Janas, J. Gurgul, R.P. Socha, S. Dzwigaj, Appl. Catal. B Environ. 91 (2009) 217–224.

[18]   R. Baran, F. Averseng, Y. Millot, T. Onfroy, S. Casale, S. Dzwigaj, J. Phys. Chem. C 118 (2014) 4143–4150.

[19]   S. Dzwigaj, P. Massiani, A. Davidson, M. Che, J. Mol. Catal. A Chem. 155 (2000) 169–182.

[20]   G. Moretti, C. Dossi, A. Fusi, S. Recchia, R. Psaro, Appl. Catal. B Environ. 20 (1999) 67–73.

[21]   M.H. Groothaert, P.J. Smeets, B.F. Sels, P. a. Jacobs, R. a. Schoonheydt, J. Am. Chem. Soc. 127 (2005) 1394–1395.

[22]   H. Praliaud, S. Mikhailenko, Z. Chajar, M. Primet, Appl. Catal. B Environ. 16 (1998) 359–374.

[23]   I. Lezcano-Gonzalez, U. Deka, H.E. van der Bij, P. Paalanen, B. Arstad, B.M. Weckhuysen, a. M. Beale, Appl. Catal. B Environ. 154-155 (2014) 339–349.

[24]   K.I. Shimizu, R. Maruyama, T. Hatamachi, T. Kodama, J. Phys. Chem. C 111 (2007) 6440–6446.

[25]   E.I. Solomon, P. Chen, M. Metz, S.-K. Lee, A.E. Palmer, Angew. Chemie Int. Ed. 40 (2001) 4570–4590.

[26]   M.H. Groothaert, J. a. Van Bokhoven, A. a. Battiston, B.M. Weckhuysen, R. a. Schoonheydt, J. Am. Chem. Soc. 125 (2003) 7629–7640.

[27]   S. Dzwigaj, J. Janas, J. Mizera, J. Gurgul, R.P. Socha, M. Che, Catal. Letters 126 (2008) 36–42.

[28]   A. Godiksen, F.N. Stappen, P.N.R. Vennestrøm, F. Giordanino, S.B. Rasmussen, L.F. Lundegaard, S. Mossin, J. Phys. Chem. C 118 (2014) 23126–23138.

[29]   J. Soria, a. Martinez-Arias, a. Martinez-Chaparro, J.C. Conesa, Z. Schay, J. Catal. 190

(2000) 352–363.

[30]   S.C. Larsen, A. Aylor, A.T. Bell, J. a. Reimer, J. Phys. Chem. 98 (1994) 11533–11540.

[31]   C.E. Sass, L. Kevan, J. Phys. Chem. 92 (1988) 14–15.

[32]   P.J. Carl, S.C. Larsen, J. Catal. 218 (1999) 208–218.

[33]   A. V Kucherov, A.N. Shigapov, A.A. Ivanov, M. Shelef, J. Catal. 186 (1999) 334–344.

[34]   A. Murali, Z. Chang, K.T. Ranjit, R.M. Krishna, V. Kurshev, L. Kevan, J. Phys. Chem. B 106 (2002) 6913–6920.

[35]   a. . Kucherov, H.. Karge, R. Schlögl, Microporous Mesoporous Mater. 25 (1998) 7–14.

[36]   J.C. Conesa, J. Soria, J. Phys. Chem. 82 (1978) 1575–1578.

[37]   G.T. Palomino, P. Fisicaro, S. Bordiga, a Zecchina, E. Giamello, C. Lamberti, J. Phys. Chem. B 104 (2000) 4064–4073.

[38]   M. Lo Jacono, G. Fierro, R. Dragone, C.N.R. Sacso, D. Chimica, V. Uni, L. Sapienza, P.A. Moro, X. Feng, J. Itri, W.K. Hall, J. Phys. Chem. B 101 (1997) 1979–1984.

[39]   K. Hadjiivanov, A. Penkova, R. Kefirov, S. Dzwigaj, M. Che, Microporous Mesoporous Mater. 124 (2009) 59–69.

[40]   S. Mintova, V. Valtchev, T. Onfroy, C. Marichal, H. Knözinger, T. Bein, Microporous Mesoporous Mater. 90 (2006) 237–245.

[41]   C. Lamberti, A. Zecchina, E. Groppo, S. Bordiga, Chem. Soc. Rev. 39 (2010) 4951–5001.

[42]   J. Szanyi, J.H. Kwak, H. Zhu, C.H.F. Peden, Phys. Chem. Chem. Phys. 15 (2013) 2368–80.

[43]   R. Kefirov, A. Penkova, K. Hadjiivanov, S. Dzwigaj, M. Che, Microporous Mesoporous Mater. 116 (2008) 180–187.

[44]   K. Frolich, R. Bulánek, E. Frýdová, Microporous Mesoporous Mater. 186 (2014) 37–45.

[45]   S. Bordiga, C. Pazé, G. Berlier, D. Scarano, G. Spoto, a. Zecchina, C. Lamberti, Catal. Today 70 (2001) 91–105.

[46]   K. Hadjiivanov, E. Ivanova, R. Kefirov, J. Janas, A. Plesniar, S. Dzwigaj, M. Che, Microporous Mesoporous Mater. 131 (2010) 1–12.

[47]   K. Góra-Marek, a. E. Palomares, a. Glanowska, K. Sadowska, J. Datka, Microporous Mesoporous Mater. 162 (2012) 175–180.

[48]   F. Giordanino, P.N.R. Vennestrøm, L.F. Lundegaard, F.N. Stappen, S. Mossin, P. Beato, S. Bordiga, C. Lamberti, Dalt. Trans. 42 (2013) 12741–61.

[49]   L. Xu, C. Shi, Z. Zhang, H. Gies, F.S. Xiao, D. De Vos, T. Yokoi, X. Bao, M. Feyen, S. Maurer, B. Yilmaz, U. Müller, W. Zhang, Microporous Mesoporous Mater. 200 (2014) 304–310.

[50]   D.L. Hoang, T.T.H. Dang, J. Engeldinger, M. Schneider, J. Radnik, M. Richter, A. Martin, J. Solid State Chem. 184 (2011) 1915–1923.

[51]   L. Xu, C. Shi, Z. Zhang, H. Gies, F.S. Xiao, D. De Vos, T. Yokoi, X. Bao, M. Feyen, S. Maurer, B. Yilmaz, U. Müller, W. Zhang, Microporous Mesoporous Mater. (2014).

[52]   R. Bulánek, B. Wichterlová, Z. Sobal, J. Tichý, Appl. Catal. B Environ. 31 (2001) 13–25.

[53]   R. Hajjar, Y. Millot, P.P. Man, M. Che, S. Dzwigaj, J. Phys. Chem. C 112 (2008) 20167–20175.

[54]   J. Dědeček, B. Wichterlová, Phys. Chem. Chem. Phys. 1 (1999) 629–637.

[55]   G. Moretti, Catal. Letters 28 (1994) 143–152.

[56]   J. Dědeček, L. Čapek, B. Wichterlová, Appl. Catal. A Gen. 307 (2006) 156–164.

[57]   B. Modén, P. Da Costa, D.K. Lee, E. Iglesia, J. Phys. Chem. B 106 (2002) 9633–9641.

[58]   C. Paolucci, A.A. Verma, S.A. Bates, V.F. Kispersky, J.T. Miller, R. Gounder, W.N. Delgass, F.H. Ribeiro, W.F. Schneider, Angew. Chemie Int. Ed. 53 (2014) 11828–11833.

[59]   R. Martínez-Franco, M. Moliner, C. Franch, A. Kustov, A. Corma, Appl. Catal. B Environ. 127 (2012) 273–280.

[60]   J. Wang, T. Yu, X. Wang, G. Qi, J. Xue, M. Shen, W. Li, Appl. Catal. B Environ. 127 (2012) 137–147.

[61]   D. Wang, L. Zhang, J. Li, K. Kamasamudram, W.S. Epling, Catal. Today 231 (2014) 64–74.

[62]   O. Mihai, C.R. Widyastuti, S. Andonova, K. Kamasamudram, J. Li, S.Y. Joshi, N.W. Currier, A. Yezerets, L. Olsson, J. Catal. 311 (2014) 170–181.

[63]   J. Eng, C.H. Bartholomew, J. Catal. 171 (1997) 27–44.

[64]   S.A. Stevenson, J.C. Vartuli, C.F. Brooks, J. Catal. 239 (2000) 228–239.

[65]   R. Baran, T. Onfroy, S. Casale, S. Dzwigaj, J. Phys. Chem. C 118 (2014) 20445–20451.

Figure Captions

Figure 1. XRD patterns recorded at room temperature of TEABEA, HAlBEA, $Cu_{2.0}$HAlBEA, spent-$Cu_{2.0}$HAlBEA, SiBEA, $Cu_{2.0}$SiBEA and spent-$Cu_{2.0}$SiBEA.

Figure 2. FTIR spectra of HAlBEA, $Cu_{2.0}$HAlBEA, SiBEA and $Cu_{2.0}$SiBEA in the OH groups range.

Figure 3. DR UV-vis spectra recorded at room temperature of $Cu_{2.0}$HAlBEA, $Cu_{2.0}$SiBEA, C-$Cu_{2.0}$HAlBEA and C-$Cu_{2.0}$SiBEA.

Figure 4. EPR spectra (298 K) of $Cu_{2.0}$HAlBEA and $Cu_{2.0}$SiBEA as synthesized then after calcination.

Figure 5. EPR spectra (77 K) of $Cu_{2.0}$HAlBEA and $Cu_{2.0}$SiBEA as synthesized then after calcination.

Figure 6. FTIR difference spectra in carbonyl stretching regions of $Cu_{2.0}$HAlBEA (A) after adsorption of a small dose (ca. 10 μmol g^{-1} (a–d) then 45 μmol g^{-1} (e–f) of CO at 100 K and (B) evolution of the spectra in dynamic vacuum at 100 K (a–g).

Figure 7. FTIR difference spectra in carbonyl stretching regions of $Cu_{2.0}$SiBEA (A) after adsorption of a small dose (ca. 10 μmol g^{-1} (a–d) then 45 μmol g^{-1} (e–f) of CO at 100 K and (B) evolution of the spectra in dynamic vacuum at 100 K (a–g).

Figure 8. TPR patterns of C-$Cu_{2.0}$SiBEA and C-$Cu_{2.0}$HAlBEA.

Figure 9. NO conversion in SCR of NO with NH_3 on $Cu_{2.0}$SiBEA and $Cu_{2.0}$HAlBEA.

Figure 10. N_2 selectivity in SCR of NO with NH_3 on $Cu_{2.0}$SiBEA and $Cu_{2.0}$HAlBEA.
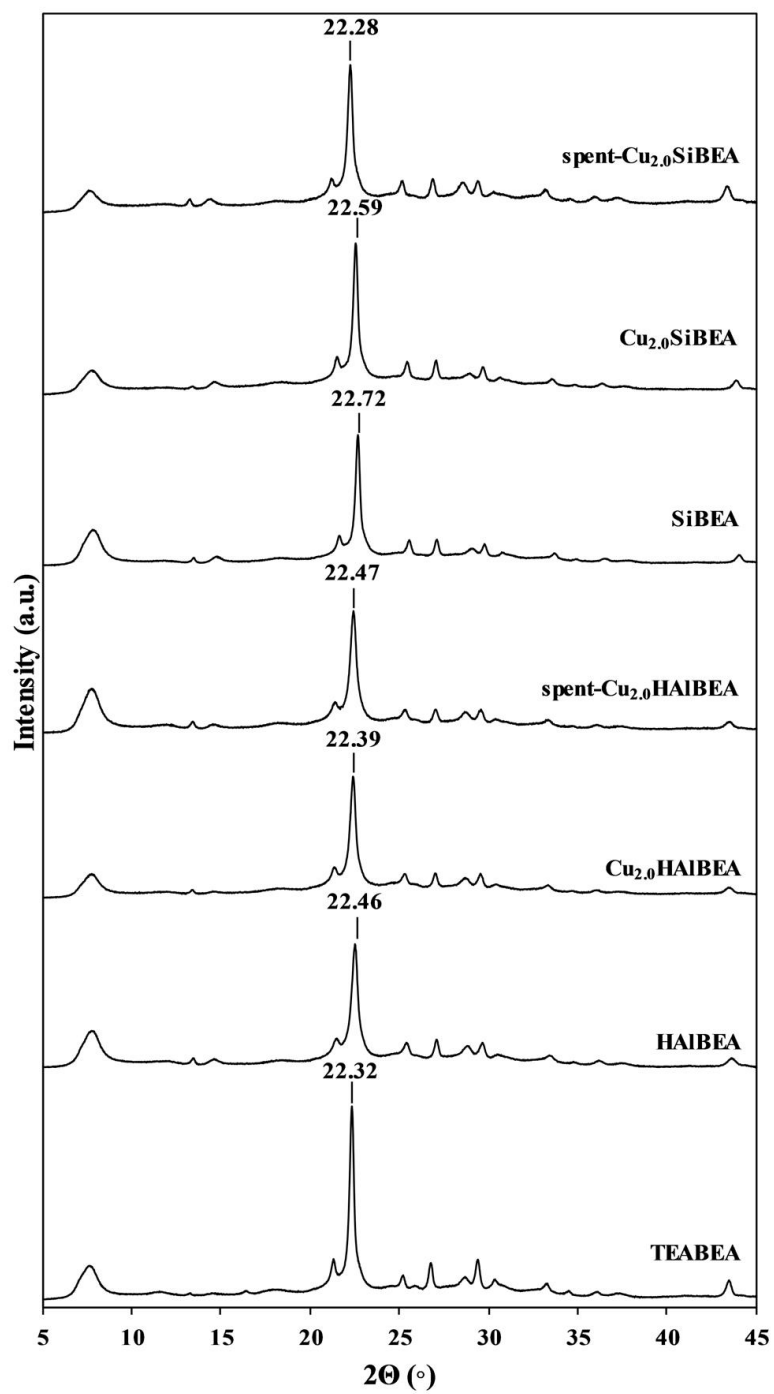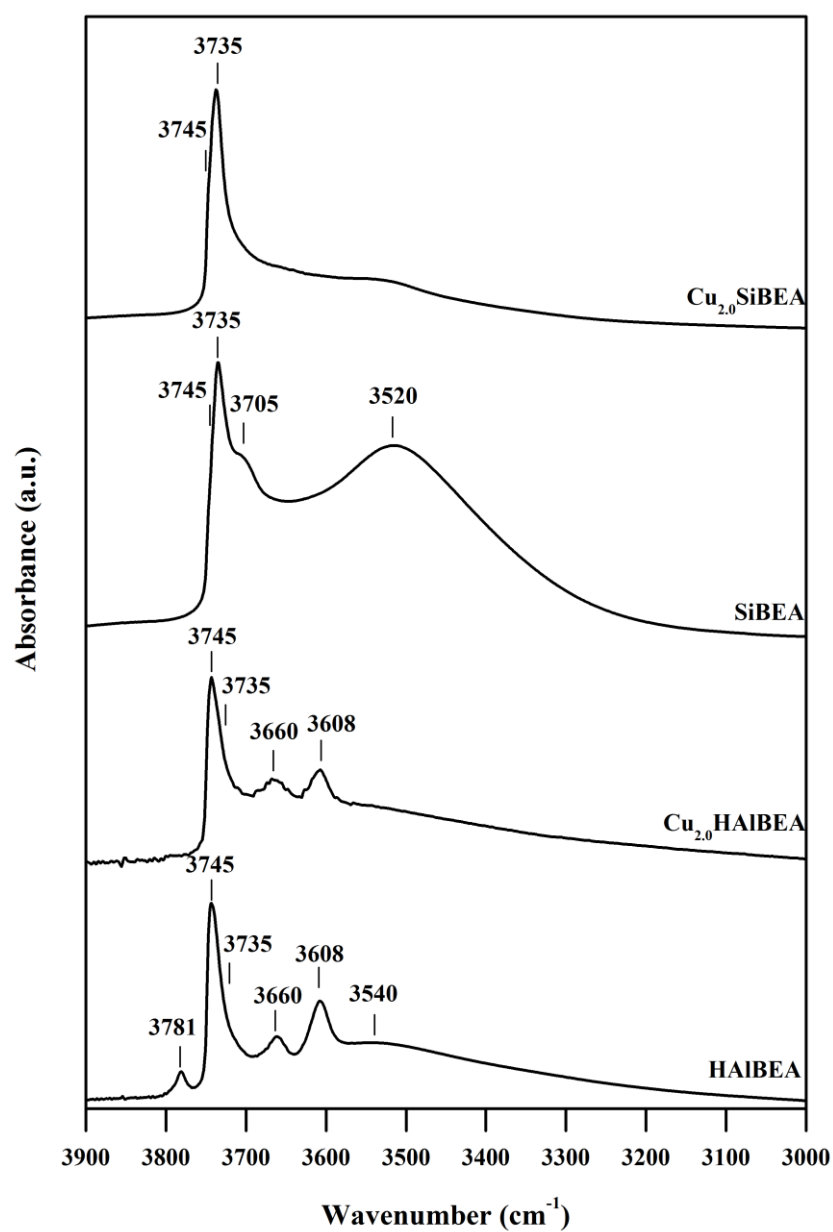
Figure 1

Figure 2
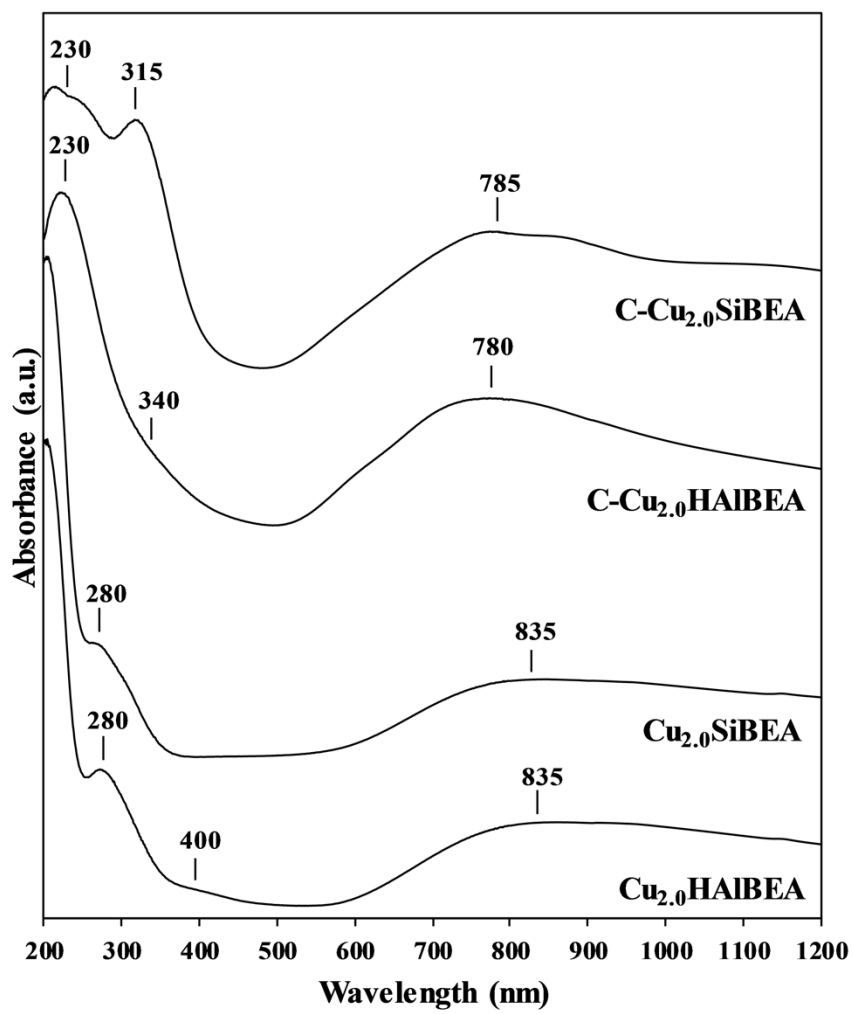
Figure 3
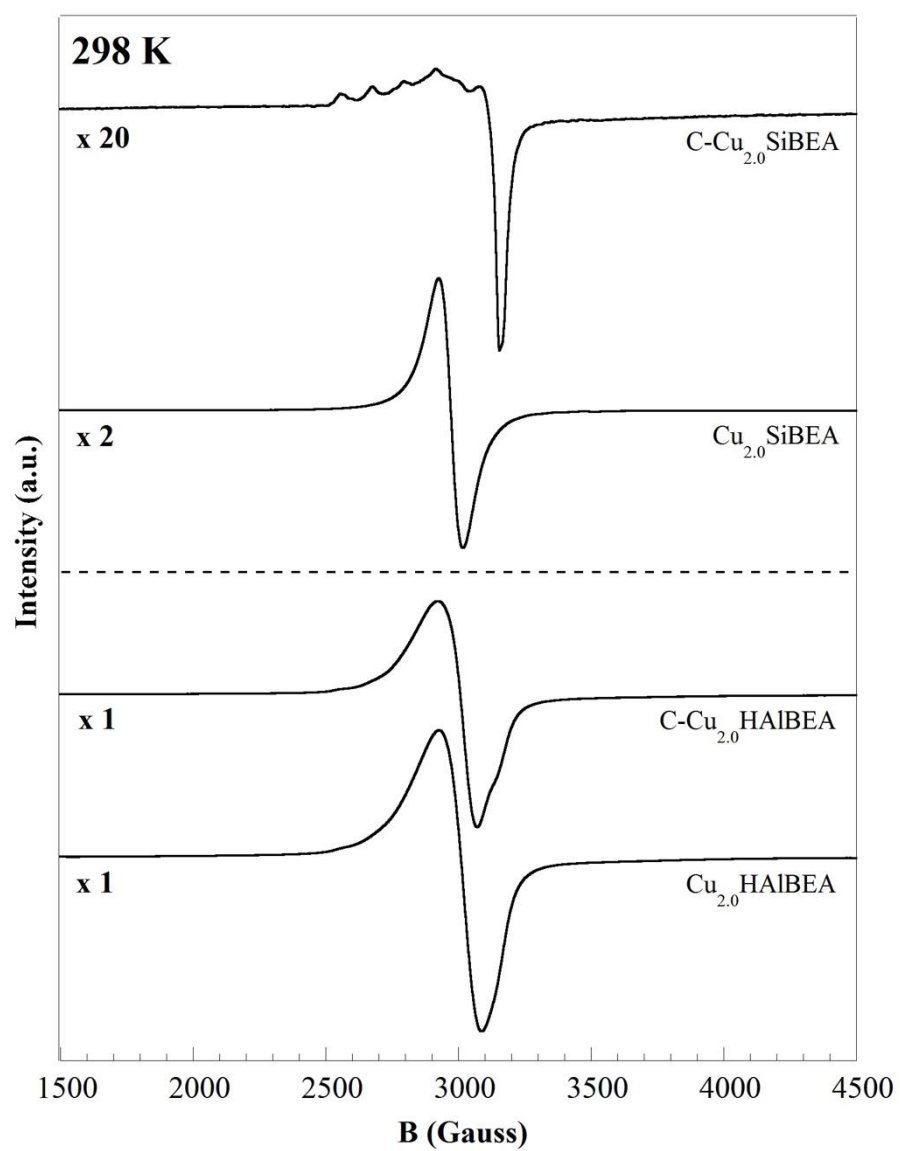
Figure 4
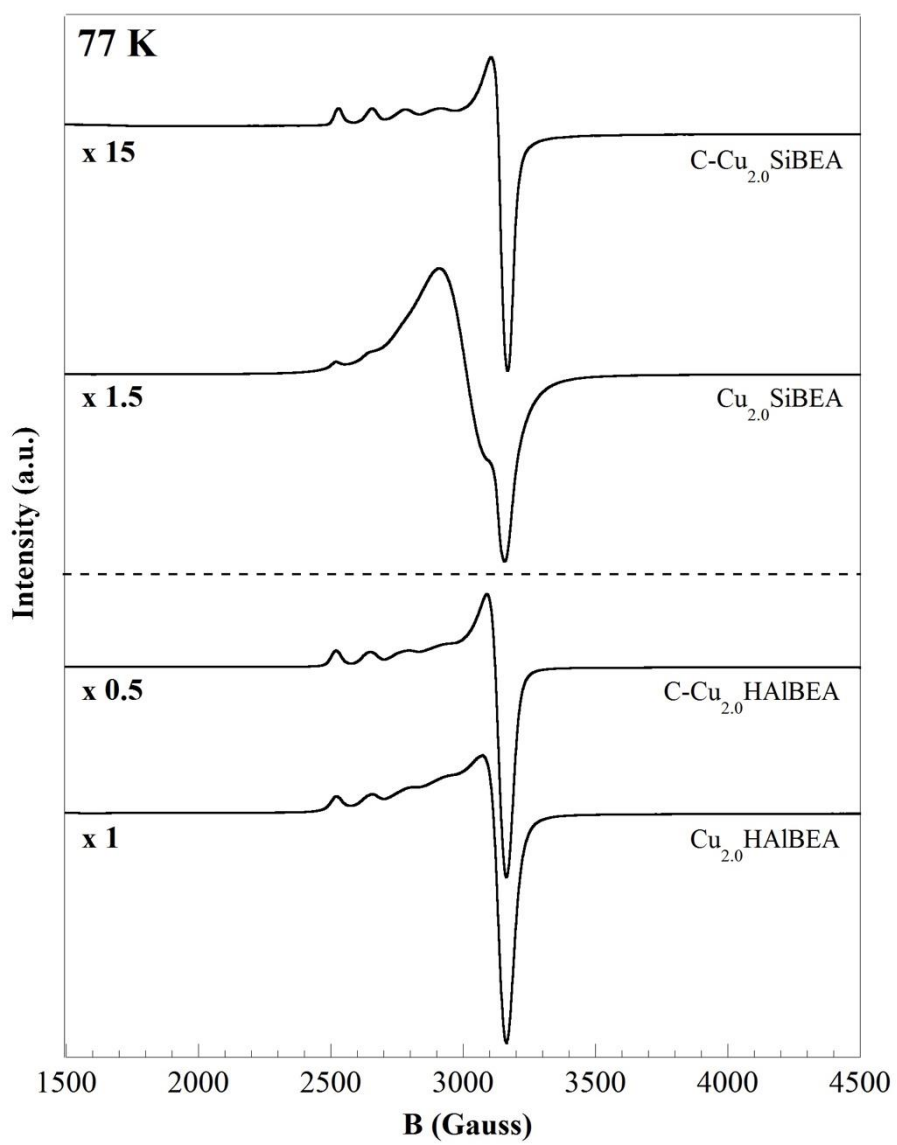
Figure 5
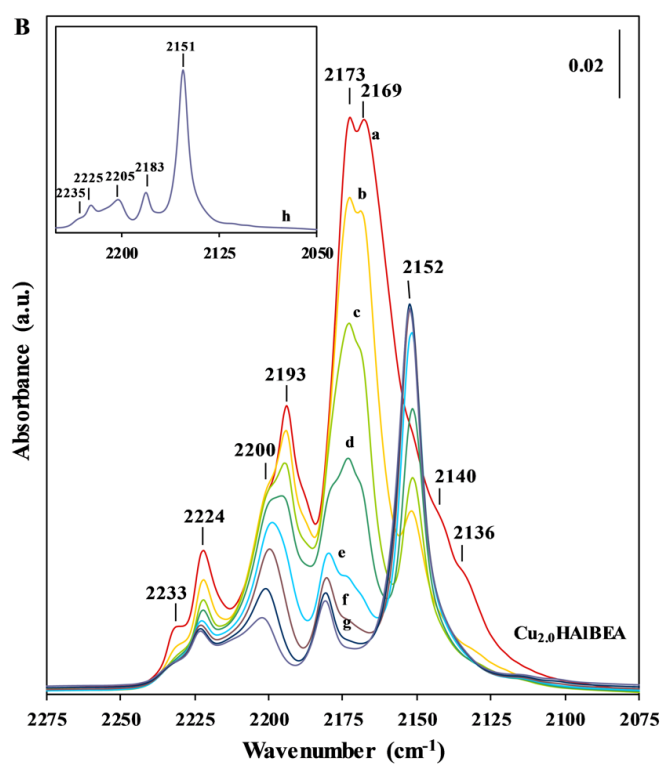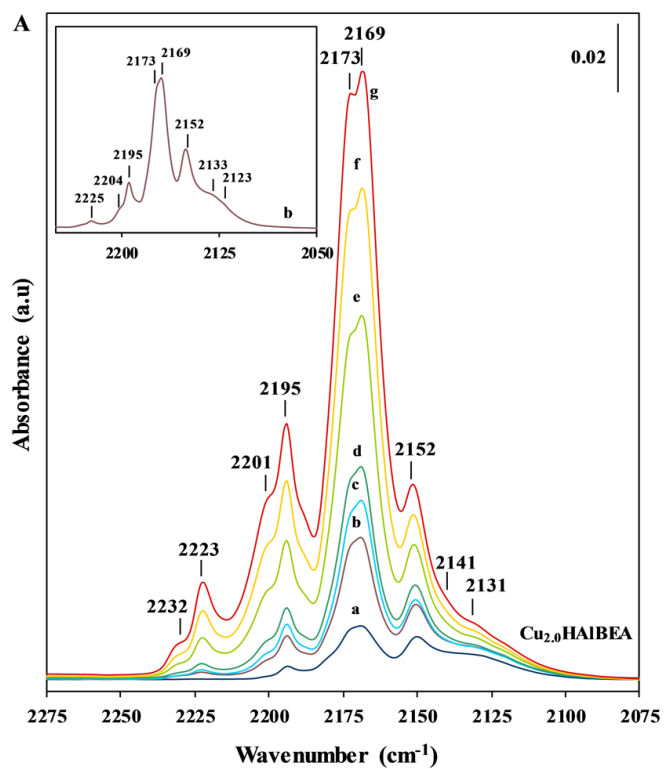
Figure 6

26
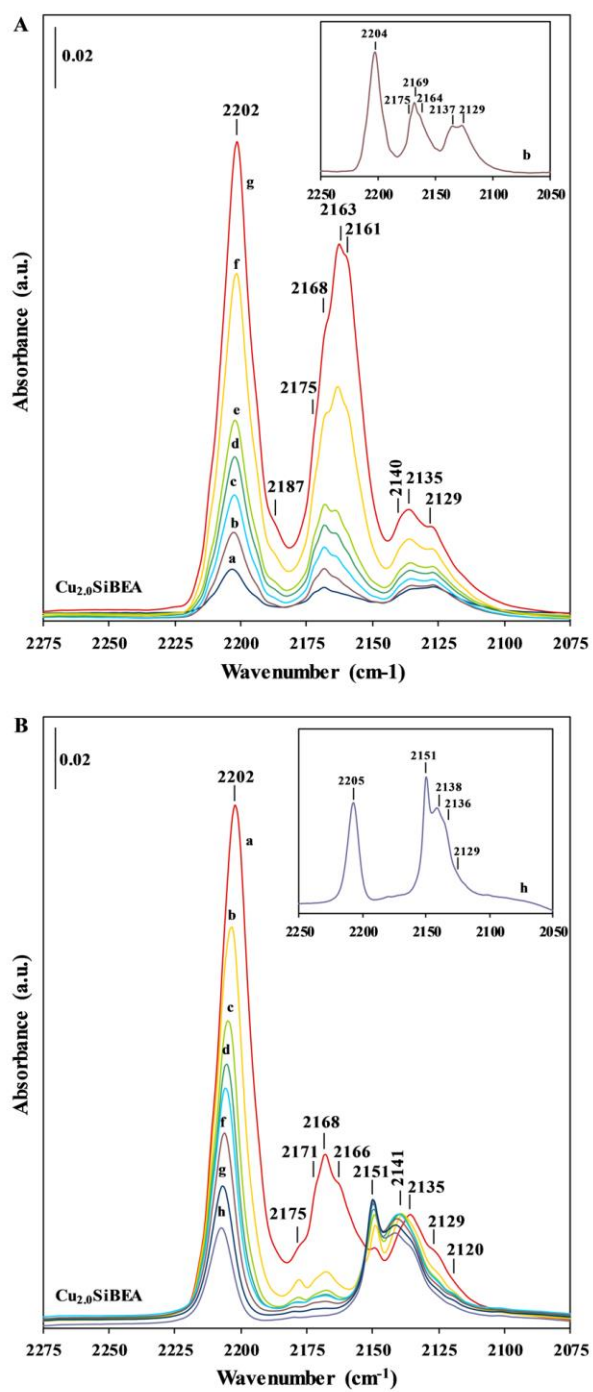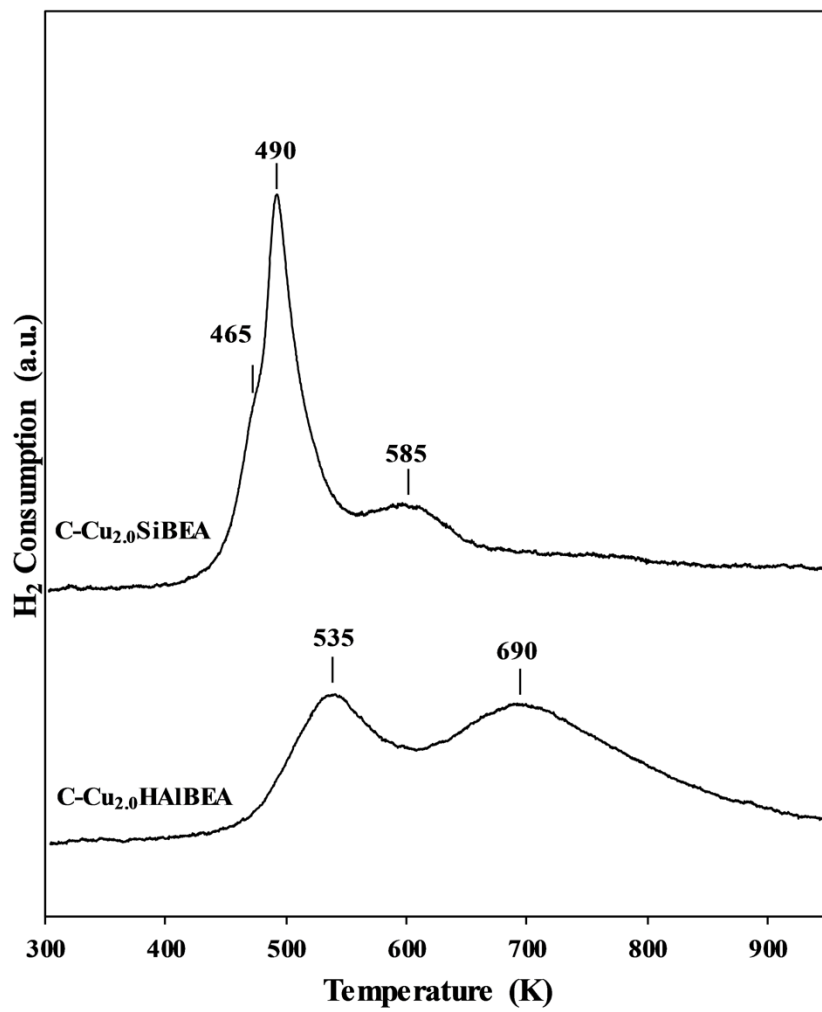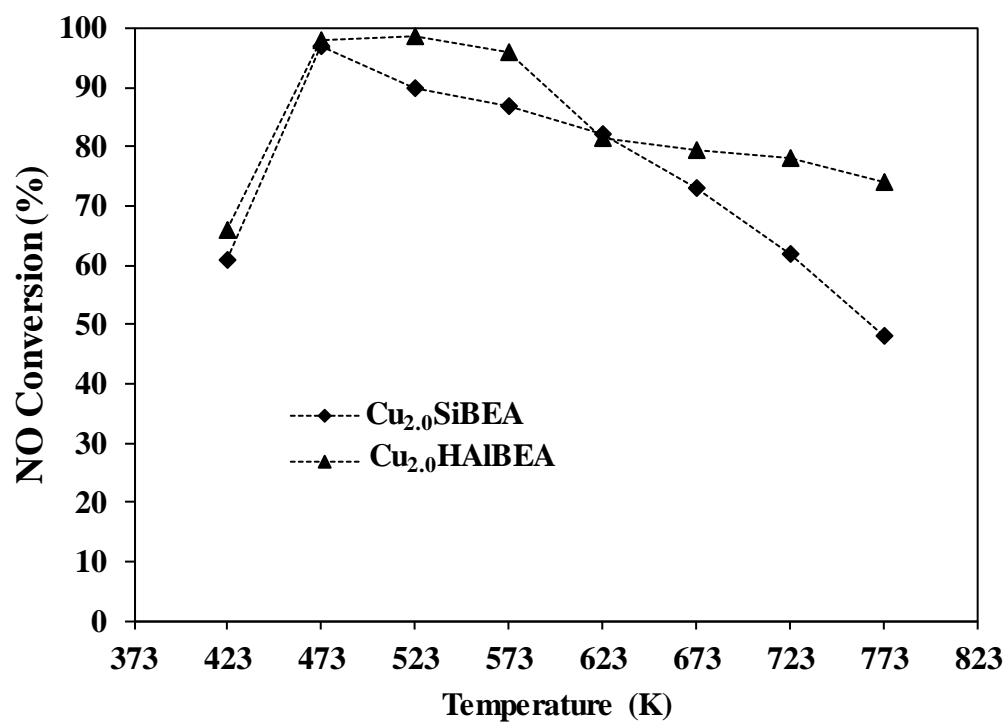
Figure 7

Figure 8

Figure 9
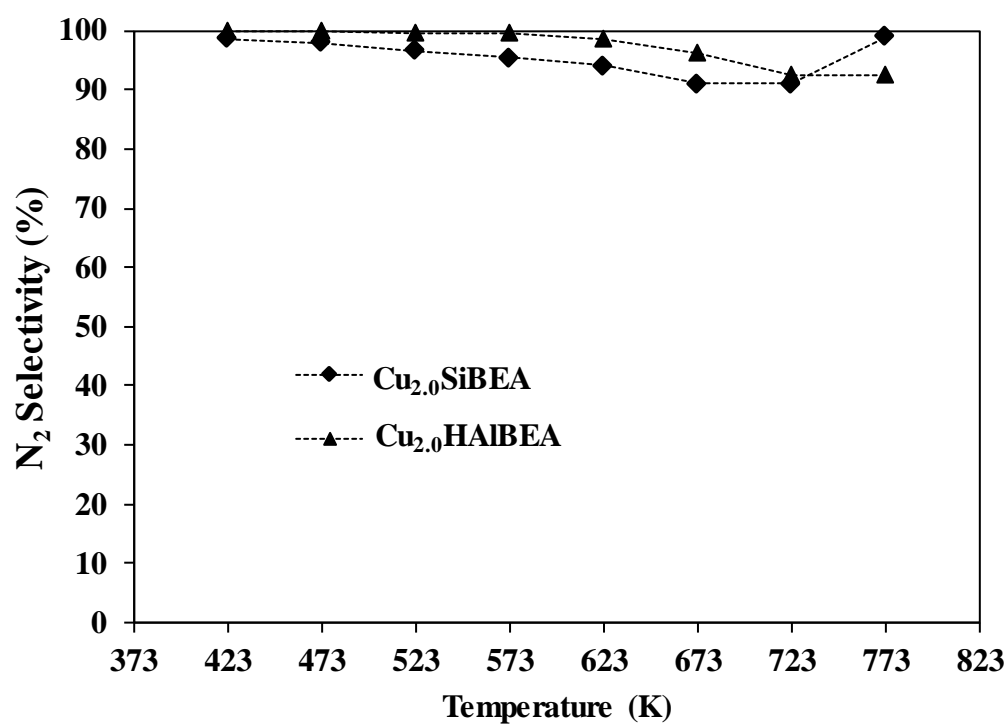
Figure 10

Table 1. Chemical composition of BEA samples.

Sample	Cu concentration (wt. %)	Si/Al ratio
TEABEA	-	17
HAlBEA	-	20
Cu$_{2.0}$HAlBEA	2.16	20
SiBEA	-	>1000
Cu$_{2.0}$SiBEA	2.18	>1000

Table 2. Simulated EPR parameters of Cu(II) present in $Cu_{2.0}HAlBEA$ and $Cu_{2.0}SiBEA$.

Samples	Treatment	Measurement T	$g_\parallel$	$A_\parallel$ (Gauss)	$g_\perp$	Relat. Int.
$Cu_{2.0}HAlBEA$	As prepared	298 K	2.29	-	2.15	-
		77 K	2.39	135	2.08	-
	Calcined	298 K	2.26	-	2.16	Major
			2.37	135	2.08	minor
		77 K	2.39	130	2.08	-
$Cu_{2.0}SiBEA$	As prepared	298 K	2.19 (g_{iso})	-	-	-
		77 K	2.30	-	2.15	Major
			2.41	125	2.08	minor
	Calcined	298 K	2.30	-	2.10	minor
			2.38	120	2.08	Major
		77 K	2.39	125	2.07	-

* Estimated errors : g values (last digit ± 3), A‖ values (± 2 Gauss),

* A⊥ is unresolved for all experimental spectra, but estimated to 10-15 Gauss for simulation purposes

Table 3. **Amounts of Brønsted and Lewis acidic centers in HAlBEA, Cu$_{2.0}$HAlBEA, SiBEA and Cu$_{2.0}$SiBEA**

Sample	Brønsted acidic centers (μmol g^{-1})	Lewis acidic centers (μmol g^{-1})
HAlBEA	333	137
Cu$_{2.0}$HAlBEA	176	342
SiBEA	8	3
Cu$_{2.0}$SiBEA	3	52

Table 4. Percentage of copper reduction in $Cu_{2.0}SiBEA$ and $Cu_{2.0}HAlBEA$ samples calculated from TPR data

Sample	Cu content, C_{Cu} (%)	Sample mass, m_s (g)	Total surface of TPR peaks, S_s (a.u.)	Cu reduction degree, R_{Cu} (%)
$Cu_{2.0}SiBEA$	2.18	0.1150	4975	65
$Cu_{2.0}HAlBEA$	2.16	0.1134	7074	100